Applied Surface Science 400 (2017) 227–237

Contents lists available at ScienceDirect

Applied Surface Science

journal homepage: www.elsevier.com/locate/apsusc

Full Length Article

The catalytic performance and characterization of ZrO_2 support modification on CuO-CeO_2/TiO_2 catalyst for the simultaneous removal of Hg^0 and NO

Teng Wang[a,b], Caiting Li[a,b,*], Lingkui Zhao[a,b], Junyi Zhang[a,b], Shanhong Li[a,b], Guangming Zeng[a,b]

[a] College of Environmental Science and Engineering, Hunan University, Changsha 410082, PR China
[b] Key Laboratory of Environmental Biology and Pollution Control (Hunan University), Ministry of Education, Changsha 410082, PR China

ARTICLE INFO

Article history:
Received 4 September 2016
Received in revised form 2 December 2016
Accepted 24 December 2016
Available online 26 December 2016

Keywords:
ZrO_2
Elemental mercury
Nitrogen oxides
CuO-CeO_2/TiO_2
Simultaneous removal

ABSTRACT

The different addition amounts of ZrO_2 on CuO-CeO_2/TiO_2 catalyst synthesized by co-precipitation method were investigated to research the simultaneous removal of Hg^0 and NO in simulated flue gas. Results indicated that the CuCe/$TiZr_{0.15}$ catalyst exhibited the superior Hg^0 removal efficiency (72.7%) and prominent NO conversion (83.3%). Hg^0 slightly restrained the NO conversion. Except for the effect of the separate NH_3 and NO on Hg^0 removal, significances of the increased NH_3/NO ratio on Hg^0 removal and NO conversion were detected. The lower GHSV could give rise to the significant acceleration of Hg^0 and NO removal. With the existence of SO_2 and H_2O, the slightly prohibitive effect on Hg^0 and NO removal was displayed. BET, XRD, SEM, H_2-TPR, XPS, FTIR analysis were applied to characterize catalysts and the results revealed the ZrO_2 modified support on CuO-CeO_2/TiO_2 resulted in strong redox ability, great mobility of surface oxygen and growing total amount of chemisorbed oxygen and lattice oxygen, which favorably impacted on Hg^0 and NO removal. The introduction of Zr benefited great surface area, weakened crystallinity of TiO_2 and then improved the dispersion of metal oxide species. More stable Lewis acid sites to form coordinated NH_3 were generated due to ZrO_2 additive. The synergetic effect through redox equilibrium of $Ce^{3+} + Cu^{2+} \leftrightarrow Ce^{4+} + Cu^{+}$ contributed to Hg^0 removal and NO conversion. In addition, the simultaneous removal of Hg^0 and NO on CuCe/$TiZr_{0.15}$ in terms of detailed mechanism was discussed.

1. Introduction

Coal-fired power plants have become one of the leading anthropogenic emission sources and produce various air pollutants. Among, elemental mercury (Hg^0) and nitrogen oxides (NO_x) are central environmental issues, which have drawn great attention recently. It is generally known NO_x (NO, NO_2 and N_2O) generate plenty of problems, including photochemical smog, acid rain, greenhouse effects and ozone depletion [1,2]. Due to the volatility, persistence, and bioaccumulation of mercury in the environment, it is a major air toxic contaminant [3]. The US Environmental Protection Agency (USEPA) on December 16, 2011 finalized the first ever national standards and controlled the discharge of mercury and other harmful air contaminants [1,4]. Hence, mercury and NO_x emission need to be constrained nowadays.

Selective catalytic reduction (SCR) is proven to be the widely-applied technique for NO_x removal [5,6]. Various technologies have been investigated for controlling Hg^0 [1,7], among which SCR is of great interest for development. In consequence, the SCR catalysts for simultaneous removal of mercury and NO_x might be an effective approach to be investigated. The valuable process of the SCR catalysts for reducing Hg^0 and NO was suggested by some recent data. For example, CeO_2 modified V_2O_5–WO_3/TiO_2 catalysts were studied for Hg^0 oxidation under different flue gas components (NO, SO_2, NH_3) [8]. Yan et al. [9] researched Hg^0 oxidation on SCR catalysts modified by RuO_2 in lower level HCl. Li et al. [4] studied mercury conversion under SCR atmosphere (SCRA), that is, NO, NH_3 and O_2, over CuO-CeO_2/TiO_2 catalyst. Besides, a series of Ce-doped V_2O_5/TiO_2 catalysts was employed to remove Hg^0 and NO simultaneously in bench scale tests [10]. Though, the traditional commercial SCR catalysts still suffer from severe problems, such as limited active temperature window and catalyst deactivation

* Corresponding author at: College of Environmental Science and Engineering, Hunan University, Changsha 410082, PR China.
E-mail addresses: ctli@hnu.edu.cn, ctli3@yahoo.com (C. Li).

http://dx.doi.org/10.1016/j.apsusc.2016.12.192
0169-4332/

by SO_2 and H_2O [11–13]. TiO_2, as one significant and conventional support, is confined for its low resistance to sintering and surface area [14]. Our object is aimed to achieve the ideal titania-based support with optimizing thermal stability and high surface area for simultaneous removal of Hg^0 and NO_x. Although the binary support, such as Al_2O_3-TiO_2 [15], TiO_2-SnO_2 [16] CeO_2-TiO_2 [8], was found to present the improved catalytic properties, ZrO_2-doped TiO_2 support might be a better alternative to replace TiO_2 [17]. The zirconia support was reported to supply the superior dispersion of active sites and better oxidation abilities than pure TiO_2 [18]. The strong thermostability, redox properties and surface acidity on the TiO_2-ZrO_2 binary oxides were displayed [14,17,19]. The surface area of catalysts could be increased by the addition of ZrO_2 [14]. The addition of Zr can inhibit the growth of TiO_2 crystallite size [17]. Marcotte et al. [20] proved multi constituent zirconia–titania oxides exhibited unprecedented catalytic properties of NH_3-SCR after aging test. The SO_2 tolerance could also be facilitated by the weak acidity and basic sites on ZrO_2 surface [21]. Furthermore, the CeO_x-based catalysts own its high catalytic oxidation on account of its large capacity storage and redox ability [13,14,22]. CuO has been explored because of its high activity at low temperature, non-toxic and relatively low price [23]. Yao et al. [23] studied the catalytic activities, structural performance and acidic property of $CuO/Ti_{0.95}Ce_{0.05}$ for NH_3-SCR at low temperature. Cu^{2+} can enhance SCR performance at the low temperature on CeO_2–CuO catalyst [24]. Besides, there existed the interaction between Ce and Cu species, which could make for great Hg^0 removal and SCR activities. However, little research on the roles of ZrO_2 doping CuO-CeO_2/TiO_2 catalyst for simultaneous removal of Hg^0 and NO were conducted.

This study investigated the ZrO_2 modified support on CuO-CeO_2/TiO_2 catalysts prepared by co-precipitation method, which could accelerate simultaneous removal of Hg0 and NO in the simulated flue gas. The research proposed the efficiency of ZrO_2-doped catalyst on Hg^0 removal and SCR reaction in simulated flue gas. Effects of simultaneous removal of Hg^0 and NO with the changes of the adding quantity of ZrO_2 and reaction conditions (Hg0, NH_3/NO, GHSV, SO_2 and H_2O) of individual Hg^0 and NO removal were investigated. The physicochemical characteristics and structure properties of catalysts with Zr additive were observed and characterized using the essential characterizations including BET, XRD, SEM, XPS, H_2-TPR, and FTIR. What is more, the catalytic properties and characterization results were operated to reveal the mechanisms of simultaneous removal of Hg^0 and NO over CuO-CeO_2/TiO_2-ZrO_2 catalyst.

2. Experimental part

2.1. Preparation of catalyst

The co-precipitation method was applied to prepare TiO_2-ZrO_2 composite oxide carriers. The desired amount of Ti $(SO_4)_2$, $ZrOCl_2{\cdot}8H_2O$ were dissolved in the deionized water with continuous stirring for 1 h which was thoroughly dissolved and presented uniform mixing. After that, the ammonia solution was added dropwise into the obtained solution under vigorously whisking at room temperature until the pH of solution arrived at 10 and the solution was continued to be stirred for 3 h. The precipitate, after air aging for 24 h at room temperature, was collected by filtration subsequently and dried overnight at 80 °C. Then the product was calcined for 5 h at 400 °C in a muffle furnace. The TiO_2-ZrO_2 carriers were defined as $TiZr_a$ (a = 0, 0.05, 0.15, 0.25, 0.35), where a represented the molar ratio of $ZrO_2/(TiO_2 + ZrO_2)$ (Zr/Ti + Zr). The support of TiO_2 or ZrO_2 was prepared likewise. The CuO-CeO_2/TiO_2–ZrO_2 (CuCe/TiZr) was prepared by the conventional impregnation method, which are detailed in supplemental materials (Part1). CuO–CeO_2/TiO_2 (CuCe/Ti), CuO–CeO_2/ZrO_2 (CuCe/Zr) catalyst was prepared with the same method.

2.2. Catalyst activity test

The simultaneous removal of Hg^0 and NO in simulated flue gas was studied with a bench-scale experimental system. As showed in Fig. 1, the simulated flue gas (SFG) consisting of 100 ug/m^3 Hg^0, 6% O_2, 500 ppm NO, 500 ppmNH_3, N_2 as the balance, was controlled by mass flow controllers (MFCs). The total flow rate of 500 mL/min was commanded, which corresponded to a gas hourly space velocity (GHSV) of approximately 50000 h^{-1}. A Dynacal mercury permeation device (VICI Metronics, USA) generated 100 ug/m^3 steady Hg^0. The effects of different flue gas compositions on Hg^0 removal and NO conversion were investigated, so 0–800 ppm SO_2 and 8 vol.% H_2O were also chosen when necessary. Among them, 0–800 ppm SO_2 was controlled by MFCs and H_2O was accurately controlled by peristaltic pump and carried out by 100 mL/min pure N_2 to the inlet of the SFG. The temperature-controlled heating tape wrapped all teflon tubes that Hg^0 and water vapor got by and its temperature was maintained at 120 °C, which could prevent condensation of Hg^0 and water vapor. Each test containing 500 mg catalyst was performed in a temperature controlled tubular furnace in the temperature window of 100–350 °C and the catalyst was packed into continuous flow quartz reactor with an inner diameter of 10 mm. The concentration of Hg^0 and NO in the gas was respectively detected by an online RA–915 M mercury analyzer (LUMEX Ltd, Russia) and a flue gas analyzer (MGA5, Germany). The outlet Hg^0 concentration was measured within the 2 h experiment, which was similar to NO concentration. Half an hour later, the relatively stable mercury concentration and NO concentration were obtained in the next tests (1.5 h). According to the average time interval (10 min) in the next 1.5 h experiment, the ten topic measured data were selected and then averaged. The error was also introduced to illustrate the credibility of data. To confirm mercury speciation, there was a mercury speciation conversion system when needed, which has been described in our previous study [25]. After this system, the flue gas ordinally entered a 10 wt% NaOH solution where acid gases were caught and a condenser where H_2O can be eliminated. The Hg^0 removal efficiency (η_{Hg}) and NO conversion efficiency (η_{NO}) were defined as the following equation, respectively:

$$\eta_{Hg}(\%) = \frac{Hg^0_{in-}Hg^0_{out}}{Hg^0_{in}} \times 100\% \quad (1)$$

$$\eta_{NO}(\%) = \frac{NO_{in-}NO_{out}}{NO_{in}} \times 100\% \quad (2)$$

Where Hg^0_{in} and Hg^0_{out} represent the inlet and outlet Hg^0 concentration ($\mu g/m^3$) respectively, NO_{in} and NO_{out} represent the inlet and outlet NO concentration (ppm) respectively. Since the mercury including both Hg^0 and Hg^{2+} went outside of reactor, partial Hg^{2+} might escape to the gas phase. The Hg^0 capture efficiency (η_{Hg^T}) was introduced to be defined as the equation below:

$$\eta_{Hg^T}(\%) = \frac{Hg^0_{in-}Hg^T_{out}}{Hg^0_{in}} \times 100\% \quad (3)$$

Where Hg^T_{out} represent the total concentration of mercury (Hg^T) ($\mu g/m^3$) at the outlet of reactor. The details of Hg^0 capture efficiency are described in supplemental materials (Part 2) (Fig. S1).

2.3. Catalyst characterization

The Brunauer–Emmett–Teller specific areas (BET) of catalysts were measured by N_2 adsorption isotherm on a Micromeritics Tris-

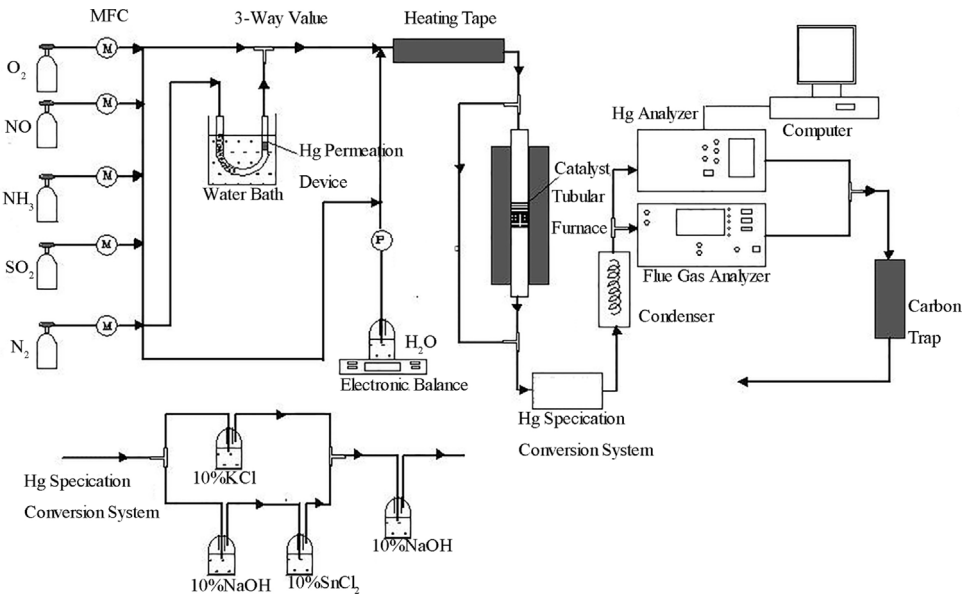

Fig. 1. Schematic diagram of the experimental setup.

tar II 3020 analyzer (Micromeritics Instrument Crop, USA). Powder X-ray diffraction (XRD) patterns of catalysts were achieved on a Rigaku D/Max 2500 system (Japan) with Cu-Ka (40 KV, 100 mA) radiation in the 2θ range from 10° to 80°. The microstructure of catalysts was investigated via scanning electron microscopy (SEM) (Hitachi S-4800, Hitachi Limited, Japan). X-ray Photoelectron Spectroscopy (XPS) was detected on a K-Alpha 1063 system (Thermo Fisher Scientific, UK) with an Al Ka X-ray source. The Temperature-programmed reduction of H_2 (H_2-TPR) was measured on an AutoChem 2920 automated chemisorption analyzer (Micromeritics Instrument Crop, USA). The Fourier Transform Infrared Spectroscopy (FTIR) was conducted on a FTIR IRInfinity-1 (SHIMADZU, Japan) apparatus. The IR spectra were recorded with 20 scans at a spectral resolution of 4 cm^{-1}. Prior to each measurement of FTIR studies, powders of the samples were grinded and mixed with KBr (200 mg, spectroscopically pure) before tableting on a hydraulic press. In order to remove any adsorbed species, the samples were pretreated at 250 °C in pure N_2 for 30 min and then cooled to room temperature with a total gas flow of 500 mL/min. The adsorption of NO + O_2 was performed at room temperature for 1 h using a gaseous feed of 500 ppm NO + 6% O_2/N_2. Subsequently, the FT-IR experiments were conducted immediately. The reaction conditions were as follows: NO + O_2 (500 ppm NO, 6% O_2/N_2), NH_3 + O_2 (500 ppm NH_3, 6% O_2/N_2), NO + NH_3 + O_2 (500 ppmNO, 500 ppmNH_3, 6% O_2/N_2), SO_2 + O_2 (300 ppm SO_2, 6% O_2/N_2) and H_2O + O_2 (8 vol.%H_2O, 6% O_2/N_2).

3. Results and discussion

3.1. Catalytic performance

3.1.1. Effect of Zr into CuCe/Ti catalysts on Hg^0 and NO removal

A comparison of a series of the CuCe/TiZr catalysts on simultaneous removal of Hg^0 and NO at 100–350 °C is shown in Fig. 2. Hg^0 removal efficiency of CuCe/TiZr catalysts increased from 100 °C to 250 °C, while it partly decreased as the temperature continued to rise to 350 °C (Fig. 2(a)). Contrasted with CuCe/Ti catalyst, the addition of Zr exhibited promotional effect on high Hg^0 removal in nearly whole temperature window and could extend the reaction window of catalyst. This enhancement of Hg^0 removal on CuCe/TiZr was consistent with its increased surface area, as showed

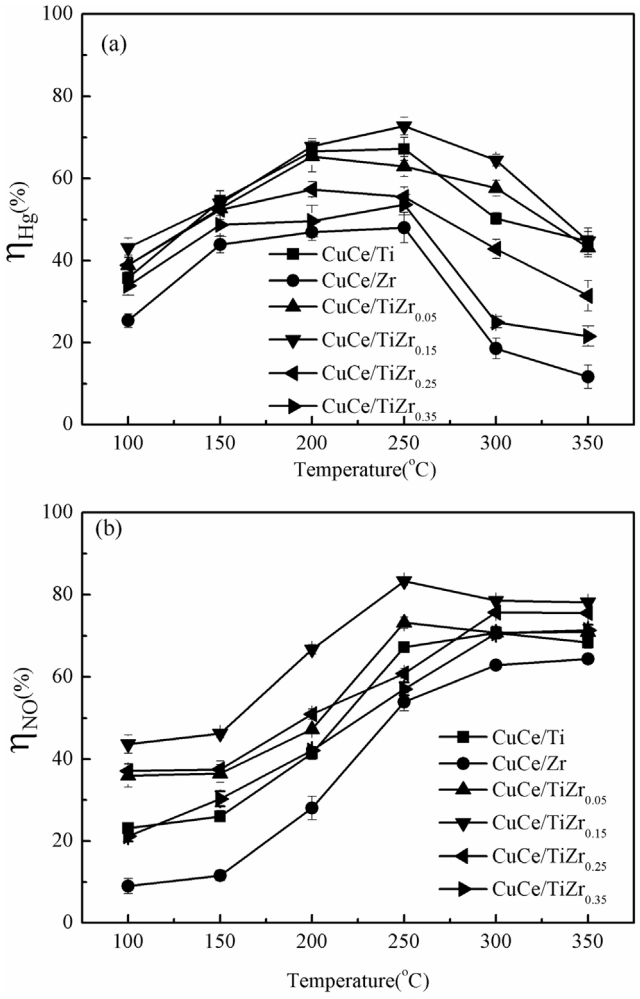

Fig. 2. Effect of Zr into CuCe/Ti catalysts on simultaneous removal of Hg^0 and NO in the simulated flue gas. Reaction condition: 100.0 μg/m^3 Hg^0, 500 ppm NO, NH_3/NO = 1, 6% O_2, N_2 as balance.

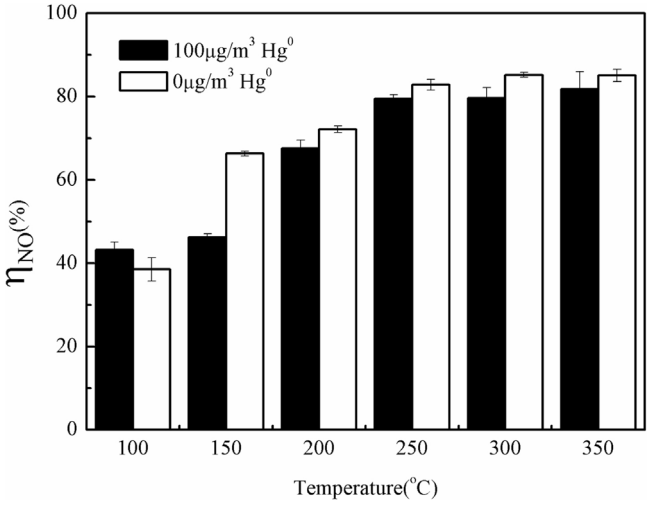

Fig. 3. Effect of Hg^0 on NO conversion on $CuCe/TiZr_{0.15}$ catalyst. Reaction condition: 0, 100.0 μg/m³ Hg^0, 500 ppm NO, NH_3/NO = 1, 6% O_2, N_2 as balance.

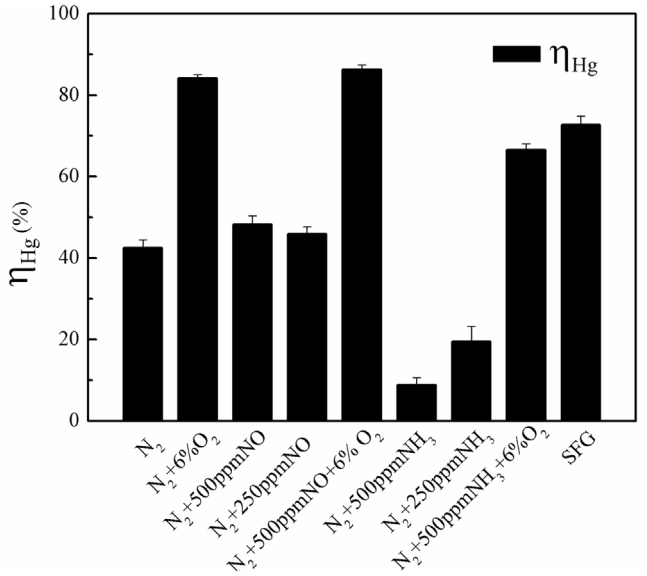

Fig. 4. Effect of NO and NH_3 on Hg^0 removal on $CuCe/TiZr_{0.15}$ catalyst respectively. Reaction condition: 100.0 μg/m³ Hg^0, 6% O_2, 250, 500 ppm NO, 250, 500 ppm NH_3 (when used), N_2 as balance, T = 250 °C.

by BET. Hg^0 removal in a wide temperature window remarkably advanced as Zr content further increased to 0.15, which could suggest that zirconia addition had restrained the efficiency loss at high temperatures [17]. When the Zr/(Ti +Zr) ratio is above 0.15, Hg^0 removal appeared lower than that observed on CuCe/Ti, especially at high temperature. It was seen in Fig. 2(b) that a higher NO conversion on $CuCe/TiZr_{0.15}$ was presented compared to CuCe/Ti and CuCe/Zr at 100–350 °C (Fig. 2(b)). NO conversion decreased slightly when Zr/(Ti + Zr) increased to 0.35. At 250 °C, $CuCe/TiZr_{0.15}$ catalyst showed the prominent Hg^0 removal efficiency (72.7%) and NO conversion (83.3%). This could be due to plenty of merits of Zr added to CuCe/Ti, that is, thermostability, high redox properties and uniform dispersion of metal oxides promoted, as characterization results indicated below and zirconia is vital to its catalytic performance. In addition, the synergetic effect between CeO_2 and CuO was conducive to effectively enhance Hg^0 and NO removal. On the Basis of the above data, Zr doping was beneficial to Hg^0 and NO removal, and $CuCe/TiZr_{0.15}$ exhibited the excellent effect of Hg^0 removal and NO conversion.

3.1.2. Effect of Hg^0 on NO conversion

Hg^0 was the central element in the simulated flue gas, which might influence the SCR catalytic activities. So the effect of Hg^0 on NO conversion of $CuCe/TiZr_{0.15}$ is investigated in Fig. 3. When gas-phase Hg^0 was got into the gas flow, NO conversion was similar with that observed in the flue gas without Hg^0. Hg^0 had slightly inhibitive effect on NO conversion probably in consequence of the relatively smaller Hg0 concentration compared to NO concentration.

3.1.3. Effect of NO and NH_3 on Hg^0 removal

This study mainly investigated the simultaneous removal of Hg^0 and NO on CuCe/TiZr catalyst, and NO and NH_3 are the most indispensable compositions in the simulated flue gas. Hence, it was vital to achieve the influence of NO and NH_3 on Hg0 removal (Fig. 4). After the introduction of 250 ppm and 500 ppm NO, Hg0 removal efficiency was 45.9% and 48.2% respectively, which were slightly higher than that of 42.5% under pure N_2. Without O_2, part of NO was reported to be weakly adsorbed on the catalysts surface, and generate NO_x with surface oxygen [26]. Adding O_2 into N_2 + 500 ppm NO resulted in the increased Hg^0 removal efficiency (86.3%), which could be due to the oxidation of more adsorbed NO to produce ample active species and gas-phase O_2 replenished for consumed surface oxygen [4,27]. So the coexistence of NO and O_2 could promote Hg^0 removal.

As shown in Fig. 4, the addition of 250 ppm NH_3 to pure N_2 made Hg^0 removal efficiency drop to only 19.5%, which was sharply lower than that observed under pure N_2. Hg0 removal exhibited more suppressive effect with a further increase of NH_3 to 500 ppm. This might be due to the consumption of surface oxygen by NH_3 [4,28]. Gaseous NH_3 was firstly adsorbed on the catalysts surface to form coordinated NH_3 and NH_2 [8,22]. The possible process might be as follows:

$$NH_{3(g)} \rightarrow NH_{3(ad)} \quad (4)$$

$$NH_{3(ad)} + O^* \rightarrow NH_{2(ad)} + OH \quad (5)$$

Where O* was active surface oxygen of catalysts. With adding 6% O_2 to N_2 + 500 ppm NH_3, Hg^0 removal efficiency was restored to 66.6%, which could be mainly attributed to the compensation via O_2 that could alleviate the inhibition of NH_3 [28].

3.1.4. Effect of NH_3/NO ratio on Hg^0 and NO removal

The NH_3/NO ratio is of great importance to influence NH_3-SCR reaction [13]. A shortage of NH_3 may reduce NO conversion [13] while the presence of NH_3 would inhibit Hg^0 removal as indicated above. Hg^0 and NO removal of $CuCe/TiZr_{0.15}$ catalyst with the change of NH_3/NO ratio at 100–350 °C are studied in Fig. 5. Hg^0 removal efficiency at 250 °C decreased from 86.3% to 68.7% as NH_3/NO ratio rising from 0 to 1.2 (Fig. 5(a)). When the temperature surpassed 250 °C, Hg^0 removal efficiency decreased sharply, and sank to 22.2% with a further increase of the NH_3/NO ratio to 1.2 at 350 °C. By contrast, the absence of NH_3 led to low NO conversion (100–350 °C), and the application of NH_3/NO ratio from 0.1 to 1.2 made NO conversion increase from 39.7% to 85.2% at 250 °C (Fig. 5(b)). It was deduced that the increase of NH_3/NO ratio had pronounced effect on Hg^0 removal and NO conversion.

3.1.5. Effect of O_2 on Hg^0 and NO removal

Oxygen is an essential factor for simultaneous removal of Hg^0 and NO (Fig. 6). There was almost inappreciable Hg^0 removal without O_2, which might be mainly ascribed to the lattice oxygen of metal oxides [29]. According to H_2-TPR and XPS results analyzed below, $CuCe/TiZr_{0.15}$ owned abundant surface oxygen species

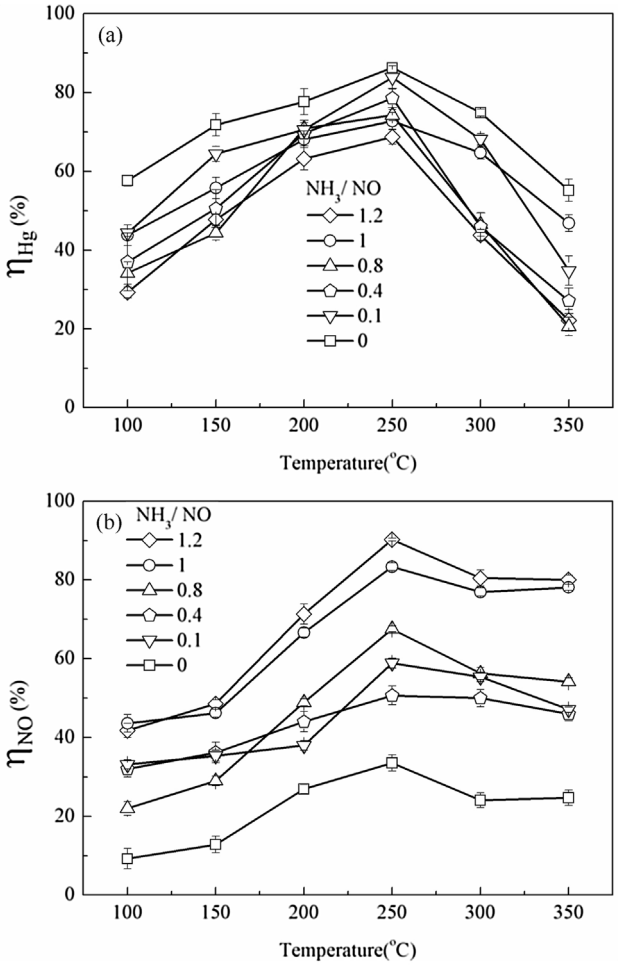

Fig. 5. Effect of NH_3/NO ratio on Hg^0 removal and NO conversion on $CuCe/TiZr_{0.15}$ catalyst. Reaction condition: 100.0 μg/m³ Hg^0, 6% O_2, 500 ppm NO, NH_3/NO = 0, 0.1, 0.4, 0.8, 1.0, 1.2, N_2 as balance.

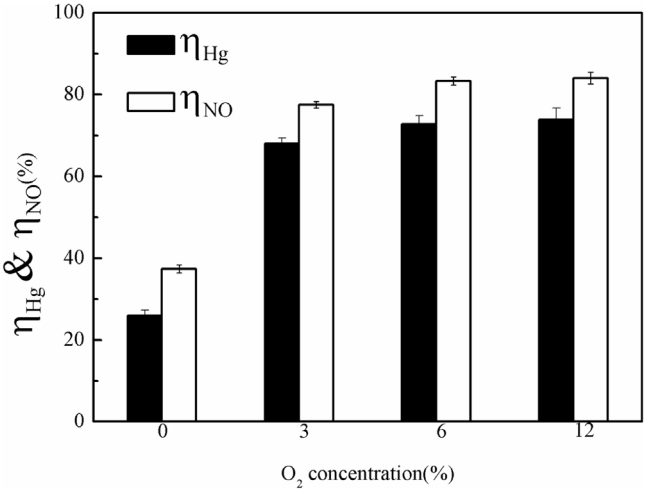

Fig. 6. Effect of O_2 on Hg^0 removal and NO conversion on $CuCe/TiZr_{0.15}$ catalyst. Reaction condition: 100.0 μg/m³ Hg^0, 500 ppm NO, NH_3/NO = 1, 0, 3, 6, 12% O_2, N_2 as balance, T = 250 °C.

and offered enough chemisorbed oxygen and lattice oxygen. Hg^0 removal efficiency with 6% O_2 was about 72.7%, which was significantly higher than that observed without O_2 (25.9%). O_2 could make the lattice oxygen regenerate and chemisorbed oxygen replenish [4]. Previous studies [29,30] had proved O_2 participated in the adsorption and oxidation of Hg^0. A negligible change of Hg^0 removal appeared after increasing O_2 concentration to 12%. NO conversion with O_2 was obviously higher than that without O_2, indicating that SCR reaction was facilitated by oxygen. Therefore, 6% O_2 for $CuCe/TiZr_{0.15}$ could be sufficient for Hg^0 and NO removal.

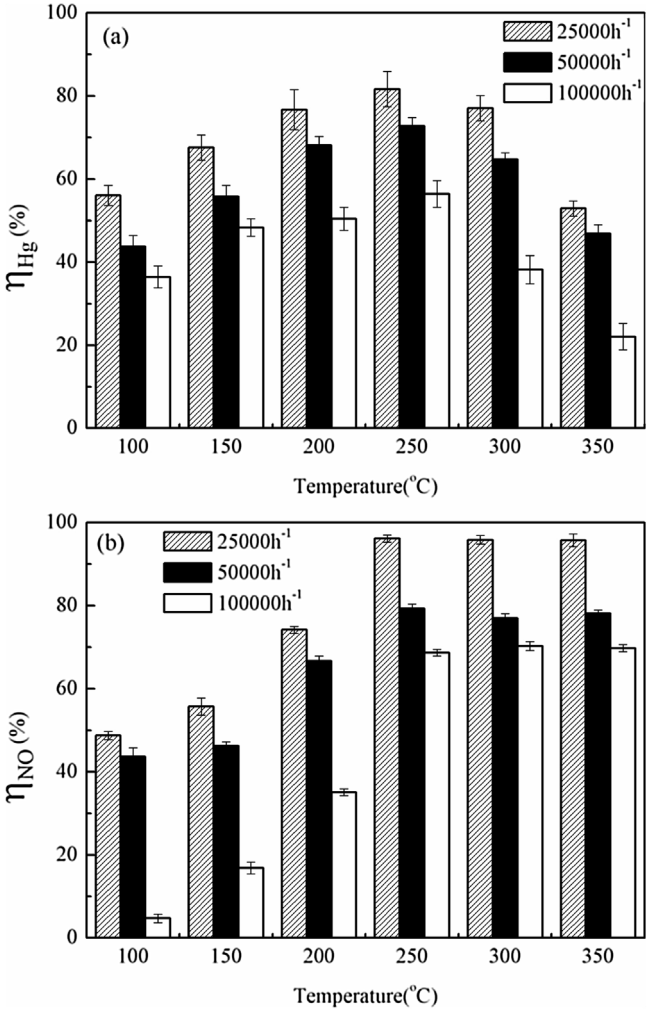

Fig. 7. Effect of GHSV on Hg^0 removal and NO conversion over $CuCe/TiZr_{0.15}$ catalyst. Reaction condition: 100.0 μg/m³ Hg^0, 500 ppm NO, NH_3/NO = 1, 6% O_2, GHSV 25000 h^{-1}, 50000 h^{-1}, 10,0000 h^{-1}, N_2 as balance.

3.1.6. *Effect of GHSV on Hg^0 and NO removal*

The performances of $CuCe/TiZr_{0.15}$ catalyst are measured in a wide GHSV range from 25000 to 100000 h^{-1}. As shown in Fig. 7(a), Hg^0 removal efficiency increased and the temperature window became broader as GHSV decreased, which could be attributed to much more contact time for catalysts exposed into reactant gases [13]. Meanwhile, NO conversion in Fig. 7(b) dramatically increased with the decreased GHSV. This suggested GHSV had prominent effect on Hg^0 and NO removal.

3.1.7. *Effect of SO_2 and H_2O on Hg^0 and NO removal*

SO_2 and H_2O are the primary constituents in flue gas, so the effects of SO_2 and H_2O over $CuCe/TiZr_{0.15}$ catalyst are considered and shown in Fig. 8. The Hg^0 removal of SO_2 was indeterminate and either promotional or inhibited [7,26]. The high Hg^0 removal efficiency could be obtained with the addition of 200 ppm SO_2 (Fig. 8(a)). However, When 800 ppm SO_2 was added to the simulated flue gas, a decrease of Hg^0 removal efficiency was observed.

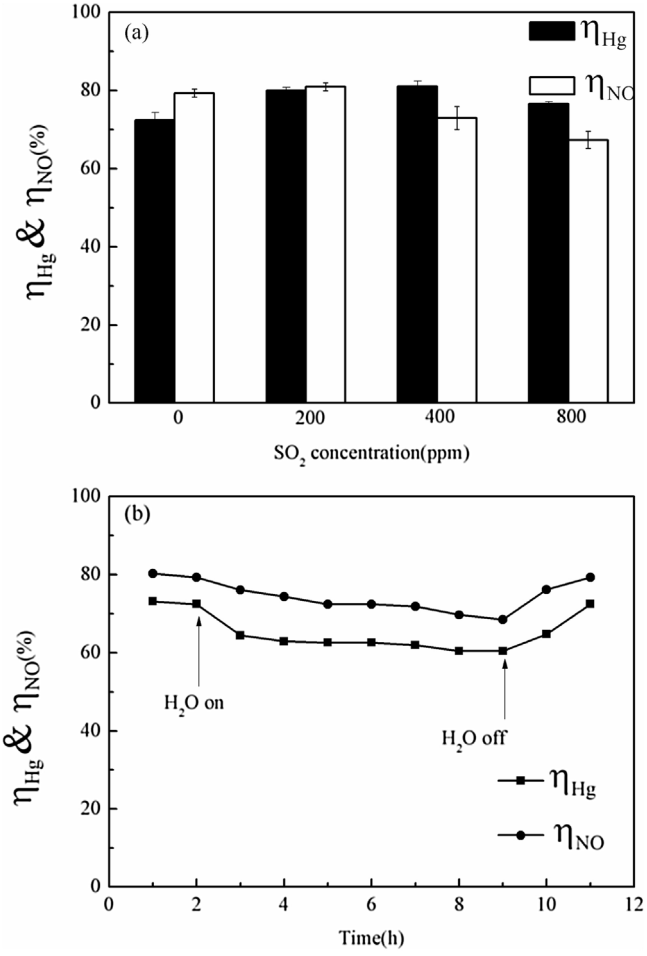

Fig. 8. Effect of SO_2 and H_2O on Hg^0 removal and NO conversion on $CuCe/TiZr_{0.15}$ catalysts. Reaction condition: 100.0 μg/m³ Hg^0, 500 ppm NO, NH_3/NO = 1, 6% O_2, N_2 as balance, T = 250 °C, (a) 0, 200, 400, 800 ppm SO_2, (b) 8 vol.% H_2O.

During the 12 h test, Hg^0 removal efficiency of 800 ppm SO_2 could be maintained in the initial stage and gradually decreased over time (in the supplemental materials) (Fig. S2). The results suggested that SO_2 might possess both promotional and inhibitive effects on Hg^0 removal, which was associated with the SO_2 concentration level [31]. Simultaneously, NO conversion of 800 ppm SO_2 was 12% lower than without SO_2. It markedly decreased in the beginning and later achieved steady state. This was in agreement with the previous study [32]. In NH_3-SCR reaction with the existence of SO_2, several kinds of sulfate species might be formed and reacted with ammonium. Ammonium sulfate or Ammonium bisulfate could be eventually generated which led to the sediment of ammonium sulfate or bisulfate on the surface and blockage of active sites [32–36]. When 8 vol.% H_2O vapor was introduced, Hg^0 removal efficiency dramatically decreased in the first 2 h, and later achieved steady state (Fig. 8(b)).The available active sites for mercury adsorption were occupied by H_2O, which probably led to the decrease of Hg^0 removal efficiency [37]. The addition of 8 vol.% H_2O caused an obvious decline of NO conversion, which might be related to the competitive adsorption between H_2O and NH_3/NO_x [38]. In summary, $CuCe/TiZr_{0.15}$ catalyst exhibited a degree of resistance to SO_2 and H_2O.

3.2. Structure and texture

The BET surface area and pore volume of different catalysts are summed up in Table 1. With the increased molar ratio of Zr/Ti + Zr, the surface area of a series of CuCe/TiZr catalysts obviously grew, which was higher than that observed on CuCe/Ti and CuCe/Zr. The $CuCe/TiZr_{0.15}$ catalyst showed the larger surface area among the Zr-containing catalysts, corresponding to the catalytic tests. It could be concluded that the textural properties and large surface area were strongly promoted by ZrO_2 in the favor of the great dispersion of metal oxide species.

Table 1
The surface area, pore volume and pore diameter of all the catalysts.

Catalysts	BET surface area (m^2/g)	Pore volume (cm^3/g)	Average pore diameter (nm)
CuCe/Ti	35.71	0.0661	7.41
CuCe/Zr	57.72	0.0745	5.16
$CuCe/TiZr_{0.05}$	45.95	0.0942	8.20
$CuCe/TiZr_{0.15}$	65.88	0.1160	7.04
$CuCe/TiZr_{0.25}$	71.66	0.1959	10.94
$CuCe/TiZr_{0.35}$	76.74	0.1827	9.52

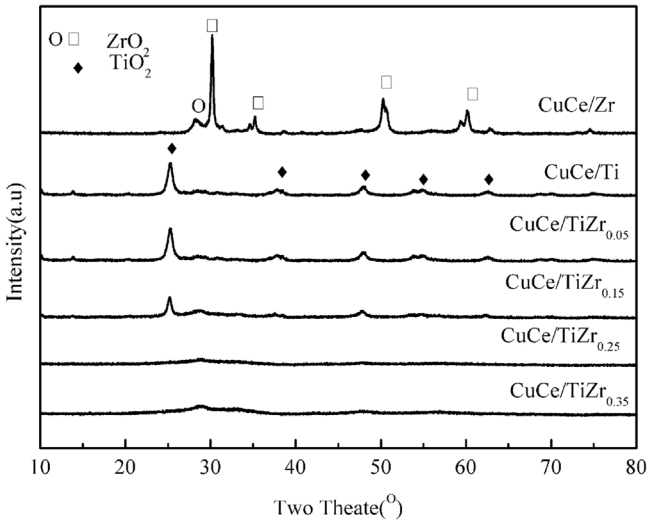

Fig. 9. XRD patterns of various catalysts.

Power XRD was conducted to study the crystal structure of all the catalysts shown in Fig. 9. There was a diffraction peak of the anatase phase at 2θ = 25.3, 37.8, 48.0, 55.0, 62.6° on CuCe/Ti [39,40], while CuCe/Zr showed the characteristic peaks of tetragonal ZrO_2 phase at 2θ = 30.2, 35.1, 50.2, 60.1° [41,42] and only one diffraction peak of momoclinic ZrO_2 phase at 2θ = 28.3° [43]. No characteristic peaks ascribed to crystalline CuO and CeO_2 could be detected, implying that copper and cerium oxides species presented high dispersion on catalyst surface. By contrast, only the diffraction peak of anatase was observed in the pattern of CuCe/TiZr catalysts. The height of halfpeak breadth of anatase on CuCe/TiZr was much lower contrasted with CuCe/Ti, suggesting that the crystal particle of anatase of CuCe/TiZr was smaller than that of CuCe/Ti. Besides, the diffraction peak observed decreased gradually and disappeared with the increased amount of ZrO_2 addition. The appropriate ZrO_2 doping could be concluded to weaken the crystallinity and reduce the crystalline size, which was probably due to the interaction between ZrO_2 and anatase support to form titanium-zirconium composite oxide. This crystallinity might transform to the amorphous structure finally. This result was in agreement with the growth of surface area, just as BET results showed. The amorphous phase could make for high concentration of active components on the surface of $CuCe/TiZr_{0.15}$, leading to the optimal Hg^0 and NO removal [44].

SEM characterizations were performed to investigate the morphology of all the catalysts shown in Fig. 10. The active species were

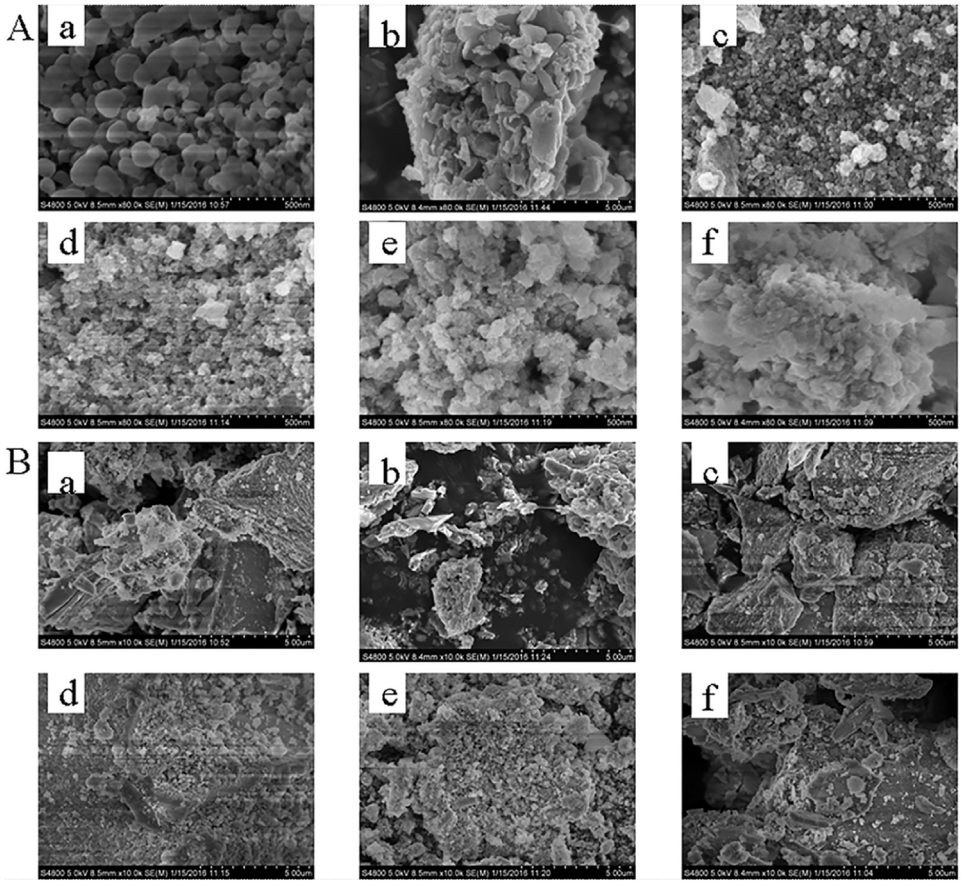

Fig. 10. SEM photographs of (a) CuCe/Ti, (b) CuCe/Zr, (c) CuCe/TiZr$_{0.05}$, (d) CuCe/TiZr$_{0.15}$, (e) CuCe/TiZr$_{0.25}$, (f) CuCe/TiZr$_{0.35}$. (A) 80,000 multiplier and (B) 10,000 multiplier.

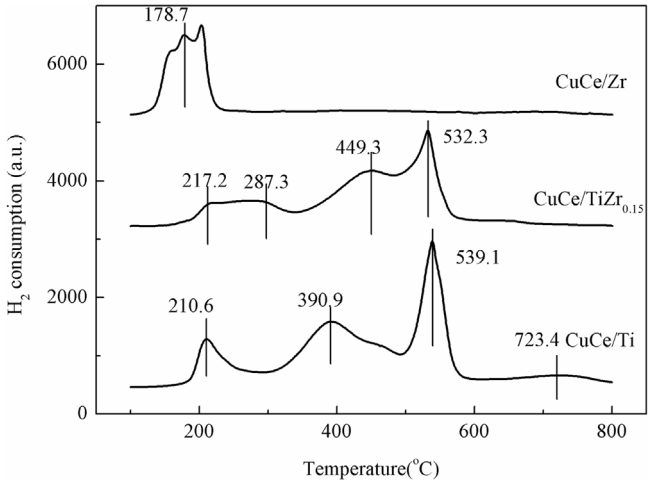

Fig. 11. H_2-TPR profiles of the CuCe/Ti, CuCe/Zr, CuCe/TiZr$_{0.15}$ catalysts.

aggregated over CuCe/Zr, whereas the large particles of CuCe/Ti deposited uniformly. The particles became small as the Zr content increased and presented the homogenous distribution. With a further increase of Zr/Ti + Zr ratio to 0.35, the particles displayed massive agglomerate. The small particles of CuCe/TiZr$_{0.15}$ presented the uniform distribution on catalyst surface, which was consistent with superior catalytic activities.

3.3. Redox properties

H_2-TPR experiments were performed in Fig. 11. Four reduction peaks centered at 210.6, 390.9, 539.1 and 723.4 °C were observed for CuCe/Ti. The peak (210 °C) showed the existence of partial copper ions on the octatomic ring window [40,45]. The peaks at 390.9, 539.1 °C were assigned to the reduction of the most easily reducible surface oxygen of ceria species [43,46]. The broad peak (723.4 °C) was due to the reduction of the release of bulk oxygen [21]. Over CuCe/Zr, a peak at around 178.7 °C was assigned to the reduction of copper species of great dispersion which significantly interacted with CeO_2 [47]. For CuCe/TiZr$_{0.15}$, the broad reduction peak from 217.2 to 287 °C corresponded to the reduction of dispersed copper oxide. Due to ZrO_2 additive, this peak shifted to the high temperature in comparison with that of CuCe/Ti [48]. The large peak of CuCe/TiZr$_{0.15}$ centered at 449.3 °C was assigned to the reduction of surface Ce^{4+} to Ce^{3+} and exhibited the low reduction temperature [38]. CuCe/TiZr$_{0.15}$ (532.3 °C) presented the lower reduction temperature than CuCe/Ti (539.1 °C), arising from great improvement of the mobility of surface oxygen. The introduction of ZrO_2 could give rise to more surface lattice oxygen and higher surface reducibility [44]. Therefore, ZrO_2 could promote the interaction of metal oxides species and then improve the redox ability of catalysts [44].

The XPS spectra of O1s, Cu 2p, Ce 3d, Zr 3d, and Hg 4f over the fresh CuCe/Ti and CuCe/TiZr$_{0.15}$ catalyst as well as used CuCe/TiZr$_{0.15}$ catalyst were investigated respectively. The O1s spectra are illustrated in Fig. 12(a). The O1s XPS spectrum was divided into three peaks. The first peak at 527.7–530.0 eV can be attributed to lattice oxygen (O_β) [43,49,50], the second peak at about 531 eV can be assigned to chemisorbed oxygen or/and weakly bonded oxy-

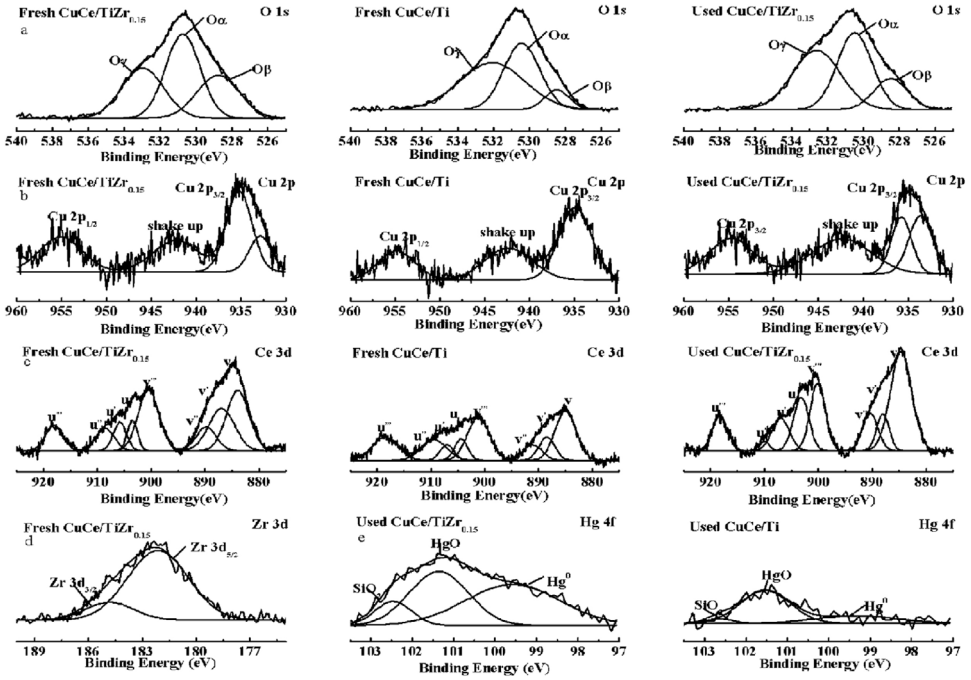

Fig. 12. XPS spectra of the fresh CuCe/Ti, fresh and used CuCe/TiZr$_{0.15}$ catalysts over the spectral regions of O 1s, Cu 2p, Ce 3d, Zr 3d, Hg 4f. Reaction condition: 100.0 μg/m^3 Hg^0, 500 ppm NO, NH_3/NO = 1, 6% O_2, N_2 as balance, T = 250 °C.

gen (O_α) [8,51], and the third peak at around 532 eV can be ascribed to hydroxyl species and adsorbed water species (O_γ) [49,52]. The ratio of $(O_\beta + O_\alpha)/O_T$ ($O_T = O_\alpha + O_\beta + O_\gamma$) of fresh CuCe/TiZr$_{0.15}$ catalyst increased compared to fresh CuCe/Ti catalyst, which might be ascribed to the production of surface oxygen species. On the contrary, the ratio of O_β/O_T and O_α/O_T decreased by 11% and 2% respectively for used CuCe/TiZr$_{0.15}$ catalyst, which indicated both O_β and O_α had participated in the oxidation [11,52]. O_2 took part in the reaction via taking up the oxygen vacancies of catalyst surface and O_β and O_α were compensated in the reaction [29].

Fig. 12(b) shows the Cu 2p spectra. It was reported [53,54] that the higher Cu 2p$_{3/2}$ band centered at 933.0–933.8 eV, the shake-up peak at 940–944 eV, and the Cu 2p$_{1/2}$ band (951–955 eV) were the primary characteristics of Cu^{2+}. Meanwhile, a lower Cu 2p$_{3/2}$ band at 932.2–933.1 eV and the inexistence of the shake-up peak were ascribed to reduced copper species. Compared to fresh CuCe/Ti catalyst, the fresh CuCe/TiZr$_{0.15}$ catalyst exhibited the appearance of a shoulder peak at 933.1 eV which was characteristic of Cu^+/Cu^0. By contrast with fresh CuCe/TiZr$_{0.15}$ catalyst, a peak of reduced copper species of used CuCe/TiZr$_{0.15}$ catalyst at 932.8 eV showed slightly broader, the reason of which might be that Cu^{2+} participated in the reaction, generating more Cu^+ species.

The obtained Ce 3d curves is shown in Fig. 12(c) The three bands labeled as v, v″ and v‴ represented Ce^{4+} 3d$_{5/2}$, while those marks as u, u″ and u‴ arose from Ce^{4+} 3d$_{3/2}$. The other two peaks labeled as u′ and v′ corresponded to Ce^{3+} species. This showed Ce^{3+} and Ce^{4+} were codependent and Ce^{4+} oxidation state was obviously predominant. However, the 25.5% ratio of Ce^{3+}/Ce^{4+} of CuCe/TiZr$_{0.15}$ was higher than 13.6% of CuCe/Ti, suggesting that the adoption of Zr benefits the generation of surface Ce^{3+}. In addition, the existence of $Ce^{3+}/(Ce^{3+} + Ce^{4+})$ was confirmed to generate a charge imbalance, more oxygen vacancies, and had powerful effects on the redox capability, adsorption capacity of NO and NH_3 [55]. Besides, the change of the ratio of Ce^{4+}/Ce^{3+} for the fresh (2.92) and used (5.06) CuCe/TiZr$_{0.15}$ catalyst might suggest Ce^{3+} participated in the oxidation reaction. Studies of CeO_2 had found its ability of storing and releasing oxygen via the redox shift ($2CeO_2 \rightarrow Ce_2O_3 + [O]$,$Ce_2O_3 + 1/2O_2 \rightarrow 2CeO_2$) [52]. This redox ability of CuCe/TiZr$_{0.15}$ might be also strongly improved by large amount of Cu^{2+} ions. The increase of Ce^{x+} oxidation state and decrease of Cu^{x+} oxidation state coexisted. The synergistic effects of copper and ceria on catalyst surface might occur, which was summarized by the equilibrium ($Ce^{3+} + Cu^{2+} \leftrightarrow Ce^{4+} + Cu^+$).

The binding energies of Zr 3d for fresh CuCe/TiZr$_{0.15}$ catalyst are recorded in Fig. 12(d). The Zr 3d spectra consisted of a doublet with Zr 3d$_{3/2}$ located at approximately 184.8 eV and Zr 3d$_{5/2}$ centered at about 182.1 eV. These peaks were assigned to Zr^{4+} [56], which was bound to a more electron attractive groups [57].

The XPS spectrum of Hg 4f level is shown in Fig. 12(e). The Hg 4f spectrum of used CuCe/Ti catalyst centered at about 99.3 and 102.6 eV, which was ascribed to Hg^0 [58] and Si 2p [29] respectively. The peak at 101.5 eV corresponded to Hg 4f for HgO [10]. This suggested that the major produce of CuCe/Ti was HgO. Besides, the binding energies of used CuCe/TiZr$_{0.15}$ catalyst centered at 99.6, 101.4 and 102.4 eV corresponded to the character of Hg^0, HgO and SiO_2 respectively [10]. The oxidized mercury formed was still mainly HgO on CuCe/TiZr$_{0.15}$. The 48.9% ratio of Hg^0 species of CuCe/TiZr$_{0.15}$ was higher than 25.1% of CuCe/Ti. This might suggest CuCe/TiZr$_{0.15}$ exhibited higher Hg^0 adsorption capacity, leading to its superior Hg^0 removal.

3.4. FTIR

FTIR spectra of adsorption on the surface of CuCe/TiZr$_{0.15}$ catalyst at room temperature for 60 min are shown in Fig. 13. The spectrum taken NO + O_2 adsorption was displayed in Fig. 13(a). The bands at 1616, 1384 cm^{-1} corresponded to adsorbed or gaseous NO_2 [59–61], and NO_3^- respectively [60]. The bands at 1192, 1112 cm^{-1} attributed to anionic nitrosyl NO^- species were observed. This was due to lanthanide metal oxides, such as CeO_2, on which NO was adsorbed [60,62] and transferred to nitrate or nitrite species. A band appeared at 1051 cm^{-1} which could correspond to nitrate species on cerium oxides [60]. A broad absorption between 3600 and 3000 cm^{-1} was due to the absorption of H-

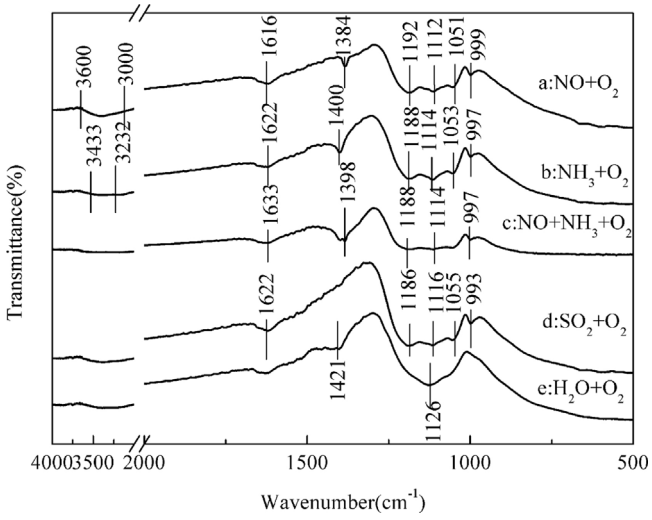

Fig. 13. FTIR spectra taken upon the CuCe/TiZr$_{0.15}$ catalyst. Reaction condition: 100.0 μg/m^3 Hg^0, 6% O_2, N_2 as balance, (a) 500 ppm NO, (b) NH_3/NO = 1, (c) 300ppmSO_2, (d) 8vol.%H_2O.

bonded hydroxyls [63]. FTIR spectra of $NH_3 + O_2$ adsorption are shown in Fig. 13(b). The strong bands at 1622, 1188, 1114 cm^{-1} were assigned to coordinated NH_3 on Lewis acid sites, while the band at 1400 cm^{-1} could be ascribed to ammonium ions (NH_4^+) on Brønsted acid sites [56,59]. The band at 1053 cm^{-1} can be assigned to coordinatively adsorbed NH_3 on Lewis sites [60]. In the NH stretching region, distinct peaks were observed at 3232, 3433 cm^{-1} [59,64]. It suggested that NH_3 can be adsorbed stably on Lewis acid sites and Brønsted acid sites. A priority for more adsorbed NH_3 was acquired by Lewis acid sites. Studied had showed [17] that ZrO_2 doping generated the decrease of peaks ascribed to Brønsted acid sites and increase of Lewis acid sites, and the latter is more stable on catalyst surface. The FTIR spectra during the coadsorption of NH_3, NO and O_2 are presented in Fig. 13(c). Different bands of 1633, 1190, 1114 cm^{-1} were ascribed to coordinated NH_3 on Lewis acid sites. The band at 1398 cm^{-1} was attributed to bridged nitrate or additional NH_4^+ ions on Brønsted sites, on account of H_2O generation during the SCR reaction [65]. This indicated NO and NH_3 could be adsorbed simultaneously. NH_3 could be firstly adsorbed during the competitive adsorption, and some NO could be oxidized to the stable bridged nitrates. As showed in Fig. 13(d), several bands were detected after coadsorption of $SO_2 + O_2$. The features at 1186 and 1055 cm^{-1} were attributed to bisulphate ion. The band at 1116 cm^{-1} was assigned to sulphate ion [66]. The band at 993 cm^{-1} may correspond to bisulphate and pyrosulphite anions [66]. The generation of sulfates or sulfites on the surface could provide new acid sites for the NH_3 adsorption and the proliferating acid sites might be mainly Lewis acid sites [51,67,68]. The band (1626 cm^{-1}) attributed to δ_{HOH} of H_2O was due to the reaction of SO_2 and surface hydroxyl groups [69]. The spectra of CuCe/TiZr$_{0.15}$ pretreated by $H_2O + O_2$ are shown in Fig. 13(e). The band at 1421 cm^{-1} in 1800–1300 cm^{-1} region corresponded to the presence of water [70]. The band at 1126 cm^{-1} might be associated with Ti–OH [17]. The slight effect on SCR activity might happen.

3.5. Mechanism for Hg^0 and NO removal over CuCe/TiZr$_{0.15}$ catalyst

According to the XPS O1 s results, both lattice oxygen ([O]) and chemisorbed oxygen ($O_{(ad)}$) took part in the reaction. Redox ability via the shift ($2CeO_2 \rightarrow Ce_2O_3 + [O], Ce_2O_3 + 1/2O_2 \rightarrow 2CeO_2$) could contain more surface lattice oxygen [52]. The redox equilibrium ($Ce^{3+} + Cu^{2+} \leftrightarrow Ce^{4+} + Cu^{+}$) could be beneficial to NH_3-SCR reaction and Hg^0 removal. Under the present circumstance, Hg^0 ($Hg^0_{(g)}$) was preferentially adsorbed on the catalyst surface, and then adsorbed Hg^0 ($Hg^0_{(ad)}$) easily interacted with active oxygen forming the adsorbed HgO ($HgO_{(ad)}$), which might partly escape into gas phase ($HgO_{(g)}$). $O_{2(g)}$ would supplement the chemisorbed oxygen and lattice oxygen, and then reoxidized the reduced metal oxides. Surface oxygen could oxidize NO to NO_2 that could react with Hg^0 to form $Hg(NO_3)_2$. The reaction of equations could be described as follows:

$$O_{2(g)} \rightarrow 2O_{(ad)} \quad (6)$$

$$2CeO_2 \rightarrow Ce_2O_3 + [O] \quad (7)$$

$$2CuO \rightarrow Cu_2O + [O] \quad (8)$$

$$2CuO + Ce_2O_3 \leftrightarrow Cu_2O + 2CeO_2 \quad (9)$$

$$Hg^0_{(g)} \rightarrow Hg^0_{(ad)} \quad (10)$$

$$Hg^0_{(ad)} + O_{(ad)} \rightarrow HgO_{(ad)} \quad (11)$$

$$Hg^0_{(ad)} + [O] \rightarrow HgO_{(ad)} \quad (12)$$

$$HgO_{(ad)} \rightarrow HgO_{(g)} \quad (13)$$

$$Cu_2O + \frac{1}{2}O_2 \rightarrow 2CuO \quad (14)$$

$$Ce_2O_3 + \frac{1}{2}O_2 \rightarrow 2CeO_2 \quad (15)$$

For NH_3-SCR, Lewis acid sites (L^*) acted as crucial active sites at low temperature. Ammonia coordinated to L^* and nitro compounds were served as the preponderant species. The adsorbed NH_3 ($NH_{3(ad)}$) would react with gaseous NO and adsorbed NO_2 that generated at the surface to form N_2. In addition, NH_4^+ ions on Brønsted sites could react with NO, which was converted into N_2 finally. On the Basis of XPS and FTIR data as well as the earlier reports [71], the possible mechanism for NH_3-SCR can be depicted as follows:

$$O_{2(g)} \rightarrow 2O_{(ad)} \quad (6)$$

$$NO + O_{(ad)} \rightarrow NO_{2(ad)} \quad (16)$$

$$NH_{3(g)} \rightarrow NH_{3(ad)} \quad (17)$$

$$2NH_{3(ad)} + NO_{2(ad)} + NO_{(g)} \rightarrow 2N_2 + 3H_2O \quad (18)$$

$$NH_{3(g)} \rightarrow NH^+_{4\,(ad)} \quad (19)$$

$$2NH^+_{4\,(ad)} + NO_{2(ad)} + NO_{(g)} \rightarrow 2N_2 + 3H_2O + 2H^+ \quad (20)$$

4. Conclusions

The Zr modified support on CuCe/Ti catalyst prepared by co-precipitation was applied for simultaneous Hg^0 and NO removal. Superior Hg^0 removal efficiency (72.7%) and NO conversion (83.3%) at 250 °C on CuCe/TiZr$_{0.15}$ were obtained. Hg^0 had slightly inhibitive effect on NO conversion. Hg^0 removal facilitated by the addition of NO was due to the NO_X species generated from the reaction between NO and surface oxygen, while the inhibitive effect on Hg^0 removal was detected with the NH_3 addition into the flue gas. The increase of NH_3/NO ratio distinctly affected Hg^0 removal and NO conversion. Adding O_2 into simulated flue gas was a great boost for the reduction of Hg^0 and NO. The presence of SO_2 and H_2O exhibited slightly prohibitive effect on Hg^0 and NO removal. The characterization results demonstrated the properties of CuCe/TiZr$_{0.15}$ have a crucial effect on the catalytic performance of Hg^0 and NO: namely of great surface area, high dispersion of active metal oxides, TiO_2 crystallinity weakened, strong redox ability, and great mobility of surface oxygen. Both chemisorbed oxygen and lattice oxygen contributed to the oxidation reaction. Besides, the more Lewis acid

sites appeared on the surfaces of CuCe/TiZr$_{0.15}$ catalyst and generation of coordinated ammonia and nitro compounds was favorable for catalytic performance. The redox equilibrium ($Ce^{3+} + Cu^{2+} \leftrightarrow Ce^{4+} + Cu^{+}$) contributed to Hg^0 removal and NO conversion. The detailed mechanism of simultaneous removal of Hg^0 and NO on CuCe/TiZr$_{0.15}$ catalyst was proposed.

Acknowledgments

This work was financially supported by the National Natural Science Foundation of China (Grant No. 51278177, 51478173), and the Scientific and Technological Major Special Project of Changsha City in China (k1502028-31).

Appendix A. Supplementary data

Supplementary data associated with this article can be found, in the online version, at http://dx.doi.org/10.1016/j.apsusc.2016.12.192.

Reference:

[1] Y. Gao, Z. Zhang, J. Wu, L. Duan, A. Umar, L. Sun, Z. Guo, Q. Wang, A critical review on the heterogeneous catalytic oxidation of elemental mercury in flue gases, Environ. Sci. Technol. 47 (2013) 10813–10823.
[2] J. Xiang, P. Wang, S. Su, L. Zhang, F. Cao, Z. Sun, X. Xiao, L. Sun, S. Hu, Control of NO and Hg° emissions by SCR catalysts from coal-fired boiler, Fuel Process. Technol. 135 (2015) 168–173.
[3] X. Zhou, W. Xu, H. Wang, L. Tong, H. Qi, T. Zhu, The enhance effect of atomic Cl in $CuCl_2/TiO_2$ catalyst for Hg° catalytic oxidation, Chem. Eng. J. 254 (2014) 82–87.
[4] H. Li, S. Wu, C.-Y. Wu, J. Wang, L. Li, K. Shih, SCR Atmosphere Induced Reduction of Oxidized Mercury over CuO–CeO_2/TiO_2Catalyst, Environ. Sci. Technol. 49 (2015) 7373–7379.
[5] B. Shen, Y. Yao, J. Chen, X. Zhang, Alkali metal deactivation of Mn–CeO_x/Zr-delaminated-clay for the low-temperature selective catalytic reduction of NO_x with NH_3, Microporous Mesoporous Mater. 180 (2013) 262–269.
[6] Z. Liu, J. Zhu, J. Li, L. Ma, S.I. Woo, Novel Mn-Ce-Ti mixed-oxide catalyst for the selective catalytic reduction of NO_x with NH_3, ACS Appl. Mater. Interfaces 6 (2014) 14500–14508.
[7] Q. Wan, L. Duan, K. He, J. Li, Removal of gaseous elemental mercury over a CeO_2–WO_3/TiO_2 nanocomposite in simulated coal-fired flue gas, Chem. Eng. J. 170 (2011) 512–517.
[8] L. Zhao, C. Li, J. Zhang, X. Zhang, F. Zhan, J. Ma, Y. e. Xie, G. Zeng, Promotional effect of CeO_2 modified support on V_2O_5-WO_3/TiO_2 catalyst for elemental mercury oxidation in simulated coal-fired flue gas, Fuel 153 (2015) 361–369.
[9] N. Yan, W. Chen, J. Chen, Z. Qu, Y. Guo, S. Yang, J. Jia, Significance of RuO_2 modified SCR catalyst for elemental mercury oxidation in coal-fired flue gas, Environ. Sci. Technol. 45 (2011) 5725–5730.
[10] X. Zhang, C. Li, L. Zhao, J. Zhang, G. Zeng, Y.e. Xie, M.e. Yu, Simultaneous removal of elemental mercury and NO from flue gas by V_2O_5–CeO_2/TiO_2 catalysts, Appl. Surf. Sci. 347 (2015) 392–400.
[11] J. Yang, Q. Yang, J. Sun, Q. Liu, D. Zhao, W. Gao, L. Liu, Effects of mercury oxidation on V_2O_5–WO_3/TiO_2 catalyst properties in NH_3-SCR process, Catal. Commun. 59 (2015) 78–82.
[12] R. Guo, Q. Wang, W. Pan, Q. Chen, H. Ding, X. Yin, N. Yang, C. Lu, S. Wang, Y. Yuan, The poisoning effect of heavy metals doping on Mn/TiO_2 catalyst for selective catalytic reduction of NO with NH_3, J. Mol. Catal. A Chem. 407 (2015) 1–7.
[13] K. Cheng, J. Liu, T. Zhang, J. Li, Z. Zhao, Y. Wei, G. Jiang, A. Duan, Effect of Ce doping of TiO_2 support on NH_3-SCR activity over V_2O_5-WO_3/CeO_2-TiO_2 catalyst, J. Environ. Sci. 26 (2014) 2106–2113.
[14] Y. Zhang, X. Zhu, K. Shen, H. Xu, K. Sun, C. Zhou, Influence of ceria modification on the properties of TiO_2-ZrO_2 supported V_2O_5 catalysts for selective catalytic reduction of NO by NH_3, J. Colloid Interface Sci. 376 (2012) 233–238.
[15] M. Polat, A.M. Soylu, D.A. Erdogan, H. Erguven, E.I. Vovk, E. Ozensoy, Influence of the sol–gel preparation method on the photocatalytic NO oxidation performance of TiO_2/Al_2O_3 binary oxides, Catal. Today 241 (2015) 25–32.
[16] L. Dong, L. Zhang, C. Sun, W. Yu, J. Zhu, L. Liu, B. Liu, Y. Hu, F. Gao, L. Dong, Y. Chen, Study of the properties of CuO/VO_x/$Ti_{0.5}Sn_{0.5}O_2$catalysts and their activities in NO + CO reaction, ACS Catal. 1 (2011) 468–480.
[17] A. Shi, X. Wang, T. Yu, M. Shen, The effect of zirconia additive on the activity and structure stability of V_2O_5/WO_3-TiO_2 ammonia SCR catalysts, Appl. Catal. B 106 (2011) 359–369.
[18] M. Yung, E. Holmgreen, U. Ozkan, Cobalt-based catalysts supported on titania and zirconia for the oxidation of nitric oxide to nitrogen dioxide, J. Catal. 247 (2007) 356–367.
[19] C. Sun, J. Zhu, Y. Lv, L. Qi, B. Liu, F. Gao, K. Sun, L. Dong, Y. Chen, Dispersion, reduction and catalytic performance of CuO supported on ZrO_2-doped TiO_2 for NO removal by CO, Appl. Catal. B 103 (2011) 206–220.
[20] N. Marcotte, B. Coq, C. Savill-Jovitt, P. Bichon, R. Cavalier, R. Durand, V. Harle, R. Marques, E. Rohart, Multi-component zirconia–titania mixed oxides: catalytic materials with unprecedented performance in the selective catalytic reduction of NO_x with NH_3 after harsh hydrothermal ageing, Appl. Catal. B 105 (2011) 373–376.
[21] J. Liu, Q. Zhao, X. Li, J. Chen, D. Zhang, Structure sensitivity of selective catalytic reduction of NO with propylene over Cu-doped $Ti_{0.5}Zr_{0.5}O_{2-\delta}$ catalysts, Appl. Catal. B 165 (2015) 519–528.
[22] J. Zhou, W. Hou, P. Qi, X. Gao, Z. Luo, K. Cen, CeO_2-TiO_2 sorbents for the removal of elemental mercury from syngas, Environ. Sci. Technol. 47 (2013) 10056–10062.
[23] X. Yao, L. Zhang, L. Li, L. Liu, Y. Cao, X. Dong, F. Gao, Y. Deng, C. Tang, Z. Chen, L. Dong, Y. Chen, Investigation of the structure acidity, and catalytic performance of CuO/$Ti_{0.95}Ce_{0.05}O_2$ catalyst for the selective catalytic reduction of NO by NH_3 at low temperature, Appl. Catal. B 150–151 (2014) 315–329.
[24] R. Guo, W. Zhen, W. Pan, Y. Zhou, J. Hong, H. Xu, Q. Jin, C. Ding, S. Guo, Effect of Cu doping on the SCR activity of CeO_2 catalyst prepared by citric acid method, J. Ind. Eng. Chem. 20 (2014) 1577–1580.
[25] S. Tao, C. Li, X. Fan, G. Zeng, P. Lu, X. Zhang, Q. Wen, W. Zhao, D. Luo, C. Fan, Activated coke impregnated with cerium chloride used for elemental mercury removal from simulated flue gas, Chem. Eng. J. 210 (2012) 547–556.
[26] Y. Xie, C. Li, L. Zhao, J. Zhang, G. Zeng, X. Zhang, W. Zhang, S. Tao, Experimental study on Hg° removal from flue gas over columnar MnO_x-CeO_2/activated coke, Appl. Surf. Sci. 333 (2015) 59–67.
[27] Y. Li, P.D. Murphy, C.-Y. Wu, Development of silica/vanadia/titania catalysts for removal of elemental mercury from coal-combustion flue gas, Environ. Sci. Technol. 42 (2008) 5304–5309.
[28] H. Li, C.-Y. Wu, Y. Li, J. Zhang, Superior activity of MnO_x-CeO_2/TiO_2 catalyst for catalytic oxidation of elemental mercury at low flue gas temperatures, Appl. Catal. B 111–112 (2012) 381–388.
[29] C. He, B. Shen, J. Chen, J. Cai, Adsorption and oxidation of elemental mercury over Ce-MnO_x/Ti-PILCs, Environ. Sci. Technol. 48 (2014) 7891–7898.
[30] H. Xu, Z. Qu, C. Zong, W. Huang, F. Quan, N. Yan, MnO_x/graphene for the catalytic oxidation and adsorption of elemental mercury, Environ. Sci. Technol. 49 (2015) 6823–6830.
[31] L. Zhao, C. Li, Y. Wang, H. Wu, L. Gao, J. Zhang, G. Zeng, Simultaneous removal of elemental mercury and NO from simulated flue gas using a CeO_2 modified V_2O_5–WO_3/TiO_2catalyst, Catal. Sci. Technol. 6 (2016) 6076–6086.
[32] W. Xu, Y. Yu, Deactivation of a Ce/TiO_2 catalyst by SO_2 in the selective catalytic reduction of NO by NH_3, J. Phys. Chem. C 113 (2009) 4426–4432.
[33] J. Huang, Z. Tong, Y. Huang, J. Zhang, Selective catalytic reduction of NO with NH_3 at low temperatures over iron and manganese oxides supported on mesoporous silica, Appl. Catal. B 78 (2008) 309–314.
[34] K.J. Lee, P.A. Kumar, M.S. Maqbool, K.N. Rao, K.H. Song, H.P. Ha, Ceria added Sb-V_2O_5/TiO_2 catalysts for low temperature NH_3 SCR: physico-chemical properties and catalytic activity, Appl. Catal. B 142–143 (2013) 705–717.
[35] L. Zhang, L. Li, Y. Cao, X. Yao, C. Ge, F. Gao, Y. Deng, C. Tang, L. Dong, Getting insight into the influence of SO_2 on TiO_2/CeO_2 for the selective catalytic reduction of NO by NH_3, Appl. Catal. B 165 (2015) 589–598.
[36] Z. Wu, R. Jin, H. Wang, Y. Liu, Effect of ceria doping on SO_2 resistance of Mn/TiO_2 for selective catalytic reduction of NO with NH_3 at low temperature, Catal. Commun. 10 (2009) 935–939.
[37] J. Yang, Y. Zhao, L. Chang, J. Zhang, C. Zheng, Mercury adsorption and oxidation over cobalt oxide loaded magnetospheres catalyst from fly ash in oxyfuel combustion flue gas, Environ. Sci. Technol. 49 (2015) 8210–8218.
[38] S. Ding, F. Liu, X. Shi, K. Liu, Z. Lian, L. Xie, H. He, Significant promotion effect of Mo additive on a novel Ce-Zr mixed oxide catalyst for the selective catalytic reduction of NO_x with NH_3, ACS Appl. Mater. Interfaces 7 (2015) 9497–9506.
[39] X. Jiang, G. Ding, L. Lou, Y. Chen, X. Zheng, Catalytic activities of CuO/TiO_2 and CuO-ZrO_2/TiO_2 in NO + CO reaction, J. Mol. Catal. A Chem. 218 (2004) 187–195.
[40] X. Sun, C. Gong, G. Lv, F. Bin, C. Song, Effect of Ce/Zr molar ratio on the performance of Cu–Ce_x–Zr_{1-x}/TiO_2 catalyst for selective catalytic reduction of NO_x with NH_3 in diesel exhaust, Mater. Res. Bull. 60 (2014) 341–347.
[41] A. Kambur, G.S. Pozan, I. Boz, Preparation, characterization and photocatalytic activity of TiO_2–ZrO_2 binary oxide nanoparticles, Appl. Catal. B 115–116 (2012) 149–158.
[42] H. Xu, Q. Zhang, C. Qiu, T. Lin, M. Gong, Y. Chen, Tungsten modified MnO_x–CeO_2/ZrO_2 monolith catalysts for selective catalytic reduction of NOx with ammonia, Chem. Eng. Sci. 76 (2012) 120–128.
[43] H. Xu, Z. Fang, Y. Cao, S. Kong, T. Lin, M. Gong, Y. Chen, Influence of Mn/(Mn + Ce) ratio of MnO_x-CeO_2/WO_3-ZrO_2 monolith catalyst on selective catalytic reduction of NO_x with ammonia, Chin. J. Catal. 33 (2012) 1927–1937.
[44] B. Jiang, B. Deng, Z. Zhang, Z. Wu, X. Tang, S. Yao, H. Lu, Effect of Zr addition on the low-temperature SCR activity and SO_2 tolerance of Fe–Mn/Ti catalysts, J. Phys. Chem. C 118 (2014) 14866–14875.
[45] J. Wang, Z. Peng, H. Qiao, H. Yu, Y. Hu, L. Chang, W. Bao, Cerium-stabilized Cu-SSZ-13 catalyst for the catalytic removal of $NO_x$by NH_3, Ind. Eng. Chem. Res. 55 (2016) 1174–1182.
[46] Z. Wang, Z. Qu, R. Fan, The Al promotional effect for $Ce_{0.4}Zr_{0.6}O_2$ mixed oxides in selective catalytic oxidation of ammonia to nitrogen, Sep. Purif. Technol. 147 (2015) 24–31.

[47] S. Sun, D. Mao, J. Yu, Enhanced CO oxidation activity of CuO/CeO_2 catalyst prepared by surfactant-assisted impregnation method, J. Rare Earths 33 (2015) 1268–1274.
[48] L. Liu, J. Cai, L. Qi, Q. Yu, K. Sun, B. Liu, F. Gao, L. Dong, Y. Chen, Influence of supports structure on the activity and adsorption behavior of copper-based catalysts for NO reduction, J. Mol. Catal. A Chem. 327 (2010) 1–11.
[49] Z. Fang, B. Yuan, T. Lin, H. Xu, Y. Cao, Z. Shi, M. Gong, Y. Chen, Monolith $Ce_{0.65}Zr_{0.35}O_2$-based catalysts for selective catalytic reduction of NOx with NH_3, Chem. Eng. Res. Des. 94 (2015) 648–659.
[50] H. Li, C.Y. Wu, Y. Li, J. Zhang, CeO_2-TiO_2 catalysts for catalytic oxidation of elemental mercury in low-rank coal combustion flue gas, Environ. Sci. Technol. 45 (2011) 7394–7400.
[51] L. Qu, C. Li, G. Zeng, M. Zhang, M. Fu, J. Ma, F. Zhan, D. Luo, Support modification for improving the performance of MnO_x–CeO_y/γ-Al_2O_3 in selective catalytic reduction of NO by NH_3, Chem. Eng. J. 242 (2014) 76–85.
[52] Y. Wang, B. Shen, C. He, S. Yue, F. Wang, Simultaneous removal of NO and Hg^0 from flue gas over Mn-Ce/Ti-PILCs, Environ. Sci. Technol. 49 (2015) 9355–9363.
[53] P.-Y. Peng, I. Jin, T.C.K. Yang, C.-M. Huang, Facile preparation of hierarchical CuO–CeO_2/Ni metal foam composite for preferential oxidation of CO in hydrogen-rich gas, Chem. Eng. J. 251 (2014) 228–235.
[54] Q. Zhang, L. Xu, P. Ning, J. Gu, Q. Guan, Surface characterization studies of CuO-CeO_2-ZrO_2 catalysts for selective catalytic reduction of NO with NH_3, Appl. Surf. Sci. 317 (2014) 955–961.
[55] P. Ning, Z. Song, H. Li, Q. Zhang, X. Liu, J. Zhang, X. Tang, Z. Huang, Selective catalytic reduction of NO with NH_3 over CeO_2–ZrO_2–WO_3 catalysts prepared by different methods, Appl. Surf. Sci. 332 (2015) 130–137.
[56] F. Cao, J. Xiang, S. Su, P. Wang, L. Sun, S. Hu, S. Lei, The activity and characterization of MnO_x–CeO_2–ZrO_2/γ-Al_2O_3 catalysts for low temperature selective catalytic reduction of NO with NH_3, Chem. Eng. J. 243 (2014) 347–354.
[57] M.K. Youne, A. Ghorbel, Comparative study of the acidity of sulphated zirconia supported on alumina prepared by sol-gel and impregnation methods, J. Sol Gel Sci. Technol. 26 (2003) 677–680.
[58] W. Lee, G.N. Bae, Removal of elemental mercury (Hg(0)) by nanosized V_2O_5/TiO_2 catalysts, Environ. Sci. Technol. 43 (2009) 1522–1527.
[59] L. Chen, J. Li, DRIFT study on cerium-tungsten/titiania catalyst for selective catalytic reduction of NO_x with NH_3, Environ. Sci. Technol. 44 (2010) 9590–9596.
[60] G. Qi, R.T. Yang, R. Chang, MnO_x-CeO_2 mixed oxides prepared by co-precipitation for selective catalytic reduction of NO with NH_3 at low temperatures, Appl. Catal. B 51 (2004) 93–106.
[61] R. Jin, Y. Liu, Z. Wu, H. Wang, T. Gu, Low-temperature selective catalytic reduction of NO with NH_3 over Mn-Ce oxides supported on TiO_2 and Al_2O_3: a comparative study, Chemosphere 78 (2010) 1160–1166.
[62] M. Kantcheva, Identification, stability, and reactivity of NO_x species adsorbed on titania-supported manganese catalysts, J. Catal. 204 (2001) 479–494.
[63] N. Tang, Y. Liu, H. Wang, Z. Wu, Mechanism study of NO catalytic oxidation over MnO_x/TiO_2 catalysts, J. Phys. Chem. C 115 (2011) 8214–8220.
[64] J. Yu, Z. Si, L. Chen, X. Wu, D. Weng, Selective catalytic reduction of NO_x by ammonia over phosphate-containing $Ce_{0.75}Zr_{0.25}O_2$ solids, Appl. Catal. B 163 (2015) 223–232.
[65] W.S. Kijlstra, D.S. Brands, Mechanism of the selective catalytic reduction of NO with NH_3 over MnO_x/Al_2O_3 II. Reactivity of adsorbed NH_3 and NO complexes, J. Catal. 171 (1997) 219–230.
[66] C. Quijada, A. Rodes, J.L. Vazquez, J.M. Perez, A. Aldaz, Electrochemical behaviour of aqueous SO_2 at Pt electrodes in acidic medium. A voltammetric and in situ Fourier transform IR study Part I. Oxidation of SO_2 on Pt electrodes with sulphur-oxygen adsorbed species, J. Electroanal. Chem. 394 (1995) 217–227.
[67] H. Chang, J. Li, X. Chen, L. Ma, S. Yang, J.W. Schwank, J. Hao, Effect of Sn on MnOx–CeO_2 catalyst for SCR of NOx by ammonia: enhancement of activity and remarkable resistance to SO_2, Catal. Commun. 27 (2012) 54–57.
[68] H. Chang, J. Li, L. Ma, C. Wang, C. Liu, J.W. Schwank, Improvement of Activity and SO_2 Tolerance of Sn-Modified MnOx-CeO_2 catalysts for NH_3-SCR at low temperatures, Environ. Sci. Technol. 47 (2013) 5294–5301.
[69] W. Xu, H. He, Y. Yu, Deactivation of a Ce/TiO_2 catalyst by SO_2 in the selective catalytic reduction of NO by NH_3, J. Phys. Chem. C 113 (2009) 4426–4432.
[70] H. Cheng, Q. Liu, M. Huang, S. Zhang, R.L. Frost, Application of TG-FTIR to study SO_2 evolved during the thermal decomposition of coal-derived pyrite, Thermochim. Acta 555 (2013) 1–6.
[71] Z. Si, D. Weng, X. Wu, J. Li, G. Li, Structure, acidity and activity of CuO_x/WO_x–ZrO_2 catalyst for selective catalytic reduction of NO by NH_3, J. Catal. 271 (2010) 43–51.